SECTION III. TASK 3. COMPREHENSIVE MODEL DEVELOPMENT AND EVALUATION

Objectives

The objective of this task is to integrate advanced chemistry and physics submodels into a comprehensive two-dimensional model of entrained-flow reactors (PCGC-2) and to evaluate the model by comparing with data from well-documented experiments. Approaches for the comprehensive modeling of fixed-bed reactors will also be reviewed and evaluated and an initial framework for a comprehensive fixed-bed code will be employed after submission of a detailed test plan (Subtask 3.b).

Task Outline

This task will be performed in three subtasks. The first covering the full 60 months of the program will be devoted to the development of the entrained-bed code. The second subtask for fixed-bed reactors will be divided into two parts. The first part of 12 months will be devoted to reviewing the state-of-the-art in fixed-bed reactors. This will lead to the development of the research plan for fixed-bed reactors. After approval of the research plan, the code development would occupy the remaining 45 months of the program. The third subtask to generalize the entrained-bed code to fuels other than dry pulverized coal would be performed during the last 24 months of the program.

III.A. SUBTASK 3.A. - INTEGRATION OF ADVANCED SUBMODELS INTO ENTRAINED-FLOW CODE, WITH EVALUATION AND DOCUMENTATION

Senior Investigators - B. Scott Brewster and L. Douglas Smoot
Brigham Young University
Provo, UT 84602
(801) 378-6240 and 4326

Graduate Research Assistant - Mike Hobbs

Objectives

The objectives of this subtask are 1) to improve an existing 2-dimensional code for entrained coal combustion/gasification to be more generally applicable to a variety of coals by incorporating advanced coal chemistry submodels, advanced numerical methods, and an advanced pollutant submodel for both sulfur and nitrogen species, and 2) to validate the advanced submodels in the comprehensive code. The comprehensive code into which the advanced submodels are to be incorporated is PCGC-2 (Pulverized Coal Gasification and Combustion 2 dimensional).

Accomplishments

Work on this subtask is being accomplished under five components: 1) Evaluation and incorporation of coal reaction submodels into the comprehensive code, 2) incorporation of improved numerical solution methods, 3) incorporation of the SO_x-NO_x submodel developed under Subtask 2.g, 4) implementation of the code on computers, and 5) code evaluation. Progress during the last quarter is described below for each of these components. During the last quarter, two poster papers were presented at the Second Annual Technical Review Meeting of the Advanced Combustion Engineering Research Center on research performed under this subtask, and one peer-reviewed paper was accepted for publication (Brewster et al., 1988).

Component 1 - Evaluation and Incorporation of Coal Reaction Submodels

This component is aimed at selecting coal reaction submodels and developing methodology for incorporating them into PCGC-2. Three alternatives for incorporating the single particle model being developed by AFR under Task 2 into PCGC-2 were described in the 5th Quarterly Report (Solomon et al., 1987). The first alternative is direct integration, without modification of the treatment of turbulence-chemistry interactions, but allowing for variability in coal offgas enthalpy. This approach is referred to as the Single Solids Progress Variable (SSPV) Method. The second alternative is to extend the current treatment of turbulence-chemistry interactions to specifically account for variability in coal offgas composition. This approach is called the Multiple Solids Progress Variable (MSPV) Method. The third alternative is a new approach based on treating the gas phase turbulence in a Lagrangian reference frame with a statistical dispersion model. This approach is referred to as the Statistical Gas Dispersion (SGD) Method. Work was conducted during the last quarter on the first two methods, and progress is outlined below. In addition to the AFR coal reaction submodel based on the FG and DVC models, a coal devolatilization model

developed at The University of Utah (Grant et al., 1987) and based on percolation theory was reviewed.

Single Solids Progress Variable (SSPV) Method - The SSPV method assumes that the coal offgas elemental composition is constant and equal to the composition of the original dry, ash-free coal. Under this method, the evolved chemical species predicted by the FG model are not individually taken into account. Only the overall weight loss and enthalpy are accounted for. The assumption of constant composition allows the mixing of the offgas with the inlet gases to be tracked with only a single progress variable (mixture fraction). Turbulence/chemistry interactions are accounted for by integrating local instantaneous gas properties calculated from equilibrium over the probability density functions of the coal and inlet gas mixture fractions. Accounting for variability in the offgas enthalpy requires solving the gas energy equation.

The initial integration of the FG/DVC submodel was performed under Subtask 4.a and is described in the 5th Quarterly Report (Solomon et al., 1987). During the last quarter, the PCGC 2 code with integrated FG/DVC submodel was transferred from AFR to BYU. A standalone version of the FG/DVC model was also transferred.

The advantage of incorporating the FG/DVC model under the SSPV approach is that it allows for the increased generality of the FG/DVC model, including varying offgas enthalpy, without significantly complicating the comprehensive code. However, the approach is limited in that all elements in the coal must be assumed to evolve at the same relative rate. Allowing for independent rates requires additional progress variables or a new approach for modeling chemistry/turbulence interactions.

Multiple Solids Progress Variable (MSPV) Method - This method allows the coal offgas elemental composition to vary with extent of burnout. Hence, hydrogen can be allowed to evolve more rapidly than carbon, for example, and nitrogen can be allowed to evolve more slowly. The evolution rate of nitrogen is particularly important, because of its propensity to form nitrogen oxide in the presence of oxygen. Nitrogen evolved in fuel-rich regions of the reactor forms molecular nitrogen rather than nitrogen oxides. Hence, accurate prediction of nitrogen evolution rate from the coal is prerequisite to accurate prediction of nitrogen oxide level in the product gas.

In the MSPV method, each element may be tracked independently, or elements that evolve at similar rates may be lumped and tracked as a group. An additional progress variable is required for each additional independent element or group. The interaction of chemistry and turbulence is accounted for by integrating the instantaneous properties of the gas over the joint probability density function of all mixture fractions to calculate the time-mean properties.

The MSPV method was tested in a simple fashion with two progress variables tracking coal offgas. Code modifications to permit this calculation were described in the First Annual Report (Solomon et al., 1987). Calculations were performed for a slightly fuel-lean (6 percent excess air), swirling, diffusion-flame combustion case using the MSPV method and two progress variables to separately track coal volatiles and char oxidation offgas. The solids composition was taken to be that of Wyoming subbituminous coal. The primary and

secondary streams were both air at 519 K. The single-step rate of Solomon et al. (1986) was used for devolatilization with an ultimate yield of 40 percent. The heat of devolatilization was assumed negligible, and the residual char was assumed to be pure carbon. Enthalpies of the char offgas and coal volatiles were determined by assuming the enthalpy of pure carbon for the char offgas, and by partitioning the daf coal enthalpy using partial compositions in correlations for heating value (Perry and Green, 1984) and heat capacity (Merrick, 1983). Results are compared with those obtained using the SSPV method.

The obvious effect of separately tracking coal volatiles and char oxidation offgas, where the char is assumed to be pure carbon and the volatile yield is fixed, is to decrease the carbon content of the early offgas and increase the carbon content of the late offgas. A more subtle effect is to alter the heating value, since total offgas enthalpy must remain constant. The differences in the predictions of the SSPV and MSPV methods can be explained in light of these two effects.

Gas temperature for the combustion case is shown in Figure III.A-1. Surface plots and isotherms are shown for both the SSPV and MSPV methods. Centerline gas temperature, total (radially integrated) burnout, and centerline concentrations of oxygen and carbon dioxide are shown in Figure III.A-2. Differences between the predictions of the two methods are substantial.

The first major difference to be noted is the size and properties of the fuel-rich region behind the flame front. This region is caused by the rapid devolatilization of the coal particles and the finite rate of mixing between the primary and secondary streams. It is characterized by a depression in the temperature surface surrounded by a high-temperature ridge where the fuel/oxidizer mixture is near-stoichiometric. The fuel-rich region is much smaller and less extreme (more shallow) in the case of the MSPV method, as seen by comparing the temperature surfaces in Figures III.A-1b and III.A-1c with that in Figure III.A-1a. The smaller and less extreme fuel-rich region in the case of the MSPV method can be explained by the increased concentration of oxygen in the early total offgas compared with carbon. The lower peak temperature in the flame front and more shallow fuel-rich region for the MSPV method can also be seen in the centerline plots in Figure III.A-2a.

After passing through the stoichiometric peak at the aft edge of the fuel-rich region, the centerline temperature declines as secondary gases containing excess oxygen and nitrogen diluent mix with the primary. This decline can be seen to be steeper and more pronounced for the MSPV method, because the early offgas (richer in volatiles) has lower heating value relative to the late offgas (richer in carbon). Farther down the combustor, the temperature increases toward that of the SSPV method, as the offgas heating value increases.

The higher temperature in the region immediately aft of the fuel-rich zone affects the burnout as shown in Figure III.A-2b. The two methods are essentially indistinguishable until the point where the secondary and primary gases mix. At this point, the burnout of the SSPV method exceeds that of the MSPV method because of the higher gas temperature. Gas composition also differs significantly between the two methods. Centerline oxygen concentration (Figure III.A-2c) drops quickly to zero at the flame front as the available oxygen in

a) SSPV method

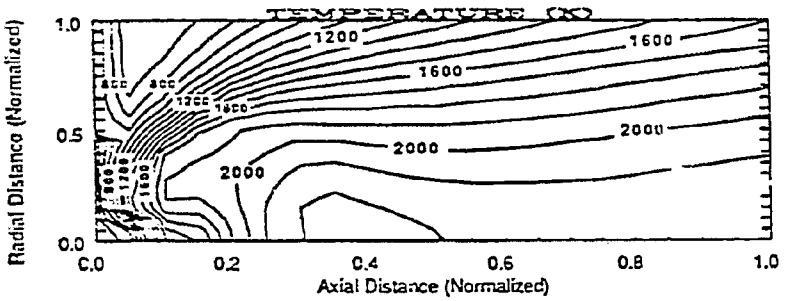

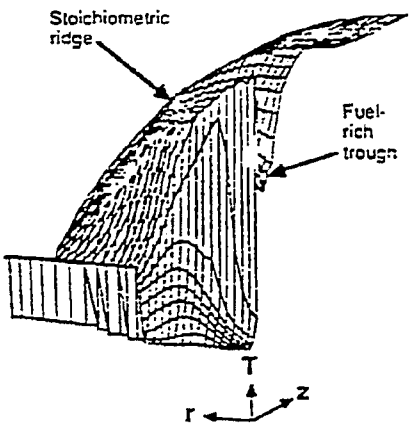

b) MSPV method (Enthalpy of char assumed to be that of pure carbon)

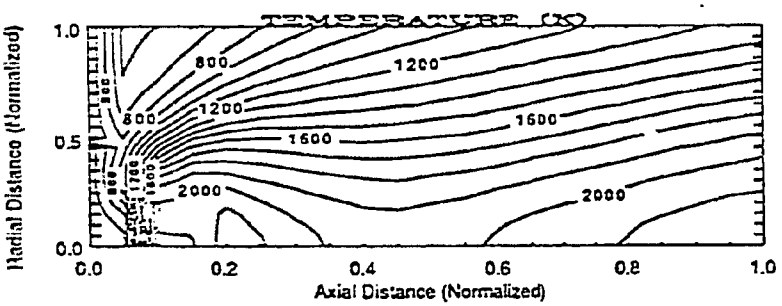

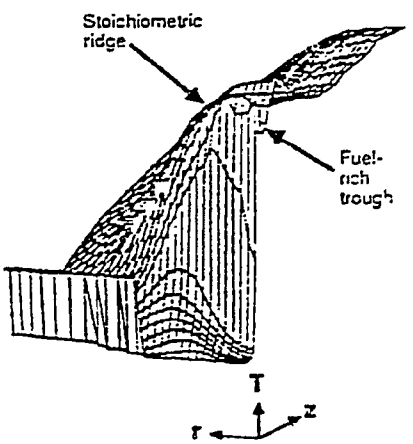

c) MSPV method (Enthalpy of char calculated from IGT correlation)

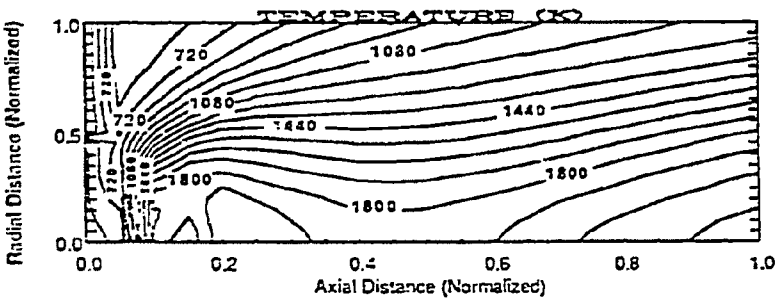

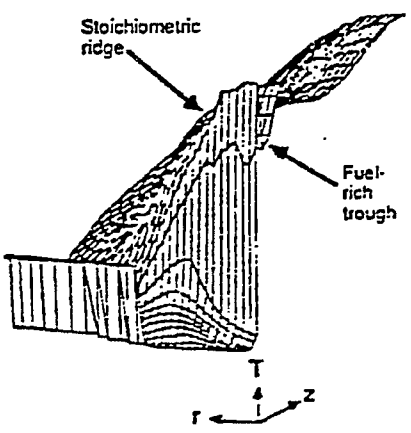

Figure III.A-1. Gas temperature isotherms and surface plots for swirled combustion case.

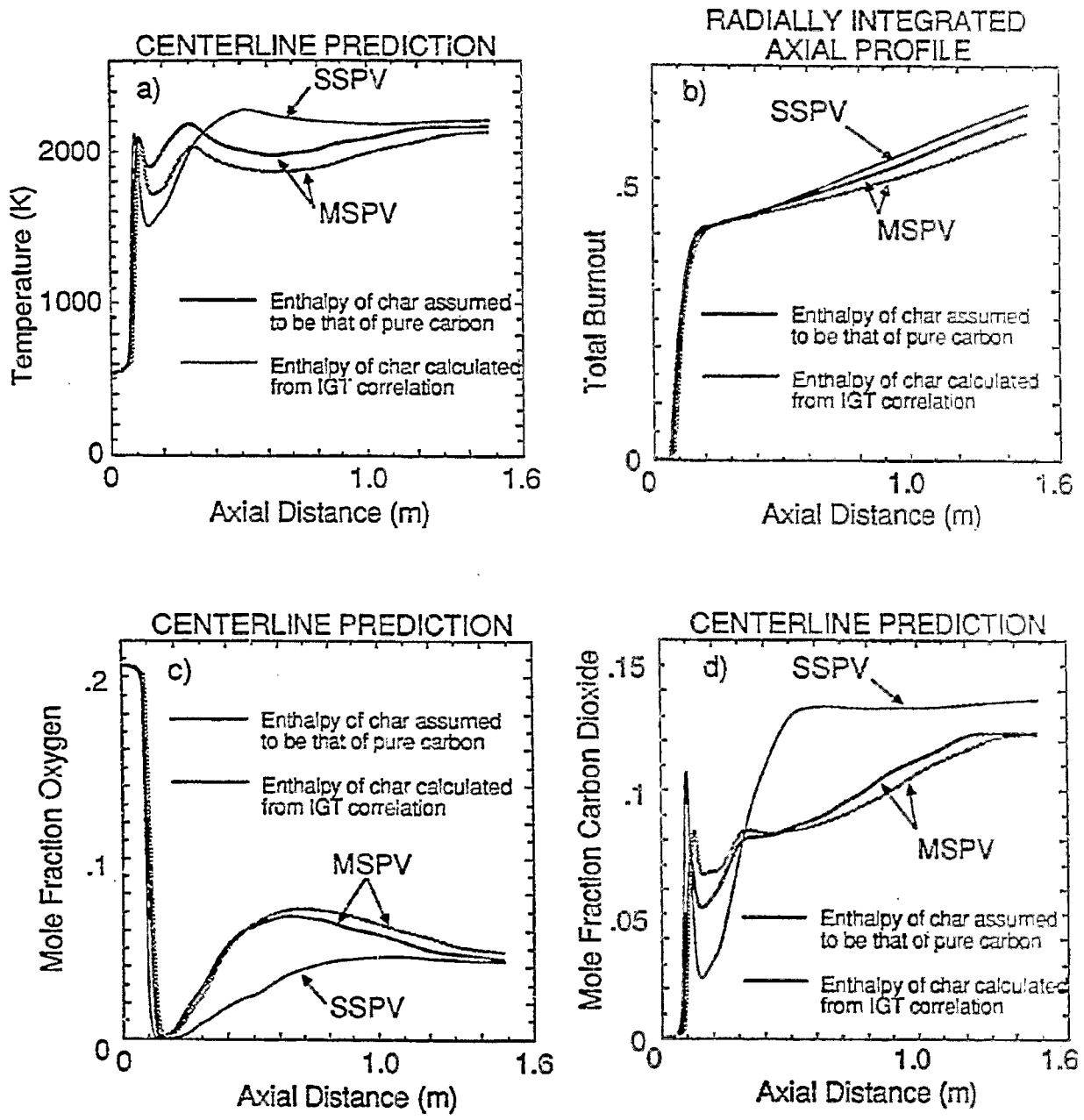

Figure III.A-2. Axial profiles for swirling combustion case.

the primary is rapidly consumed by reaction with volatiles and char. The drop is less steep for the MSPV method due to the increased content of oxygen in the early offgas. The oxygen level increases as the secondary gases mix into the center of the reactor. The increase is higher in the case of two mixture fractions because of the lower burnout.

The centerline concentration of carbon dioxide (Figure III.A-2d) rises sharply at the flame front due to reaction of oxygen with evolving carbon monoxide. It then drops in the fuel-rich region as the oxygen is depleted. The drop is less severe in the case of two mixture fractions because of the increased evolution of oxygen from the coal. The carbon dioxide concentration then increases as oxygen from the secondary stream mixes into the center of the combustor and reacts with the char. The increase is more rapid in the case of one mixture fraction because of the higher rate of burnout. The carbon dioxide profile is flat in the aft region of the reactor for the SSPV method, indicating that burnout at the centerline is essentially complete. Burnout is not complete in the center of the reactor for the MSPV method, and the carbon dioxide concentration continues to increase. The increase in total burnout in the aft region of the reactor for the SSPV method (Figure III.A-2b) must therefore be primarily due to reaction of particles near the wall. The effects of separately tracking coal volatiles and char oxidation offgas are particularly significant in this slightly fuel-lean, swirling combustion case, because of the fuel-rich zone where the particles devolatilize.

Calculations were also performed for a case simulating oxygen-blown gasification of Utah bituminous coal. The primary stream was swirled in this case, but the secondary stream was not. In addition to tracking coal volatiles and char offgas separately, a calculation was performed where all hydrogen originating from the coal was tracked with one progress variable, and all other elements originating from the coal were tracked with the other variable. A simple correlation based on experimental data was used to represent the rate of hydrogen evolution, and the evolution rate of the other elements was obtained by material balance. The assumed hydrogen evolution rate and experimental data are shown in Figure III.A-3. The assumed rate encloses most of the experimental data points and represents an upper limit to the observed rate. Isotherms and temperature surfaces for the SSPV and MSPV methods are shown in Figure III.A-4. Comparing Figure III.A-4 with Figure III.A-1 for the case of oxygen-blown gasification, the peak temperatures are much higher (well over 3000 K compared with slightly over 2000 K) and the reaction and mixing is completed in only the initial region of the reactor. These observations are typical of gasification simulations. The temperature surfaces for the SSPV and two MSPV simulations are practically indistinguishable. Slight differences can be seen in the isothermal plots.

A more quantitative comparison is shown in Figure III.A-5, where centerline gas temperature, radially integrated burnout, and centerline oxygen and carbon dioxide mole fractions are plotted as a function of axial distance. Again, little difference is noted, except for the carbon dioxide mole fraction, where the concentration for the MSPV method is less than that of the SSPV method at distances of from 0.2 to 0.5 m. At distances less than 0.2 m, the SSPV and MSPV methods are indistinguishable, and at distances greater than 0.5 m, the MSPV method is indistinguishable from the SSPV method if volatiles and char offgas are tracked separately, but less than the SSPV method if hydrogen is tracked separately. The lower value of carbon dioxide concentration in the early region

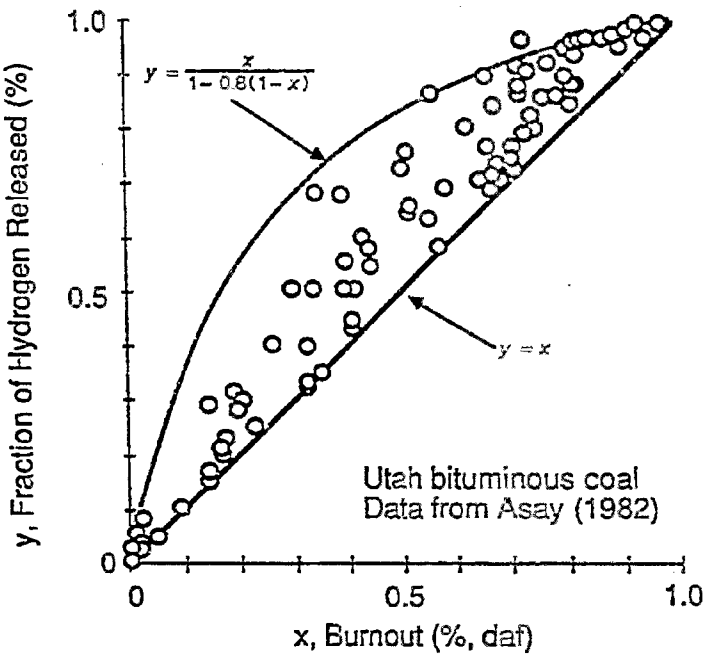

Figure III.A-3. Experimental data and limiting correlation for evolution of hydrogen as a function of burnout for Utah bituminous coal.

a) SSPV method

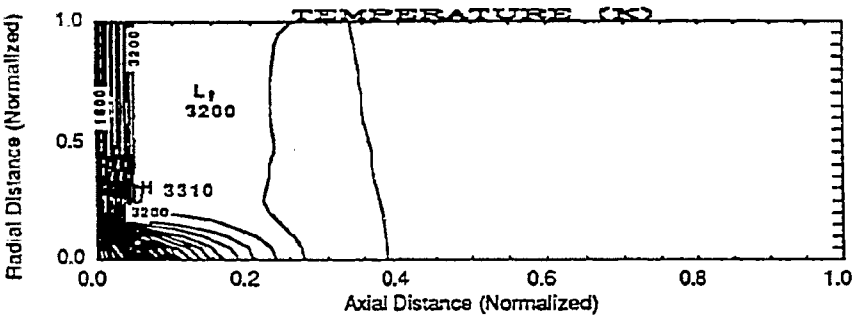

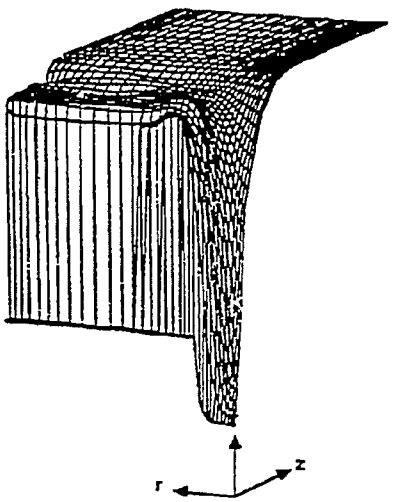

b) MSPV method (Char offgas and volatiles tracked separately)

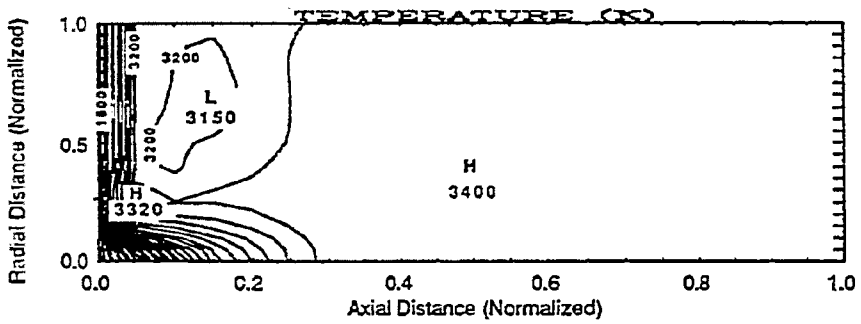

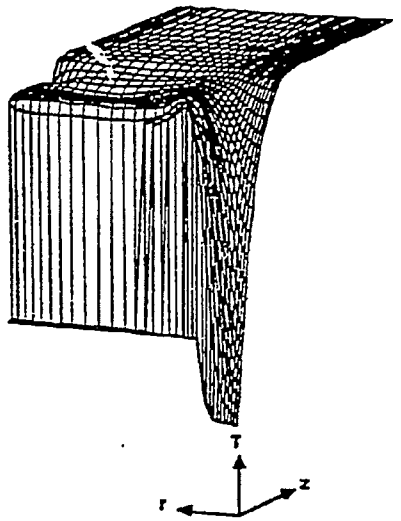

c) MSPV method (Hydrogen tracked separately)

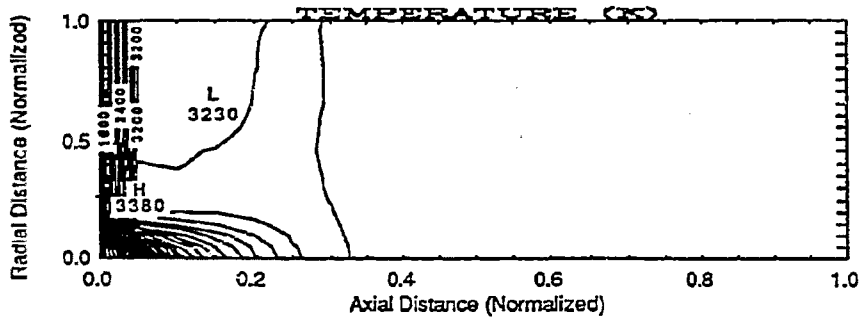

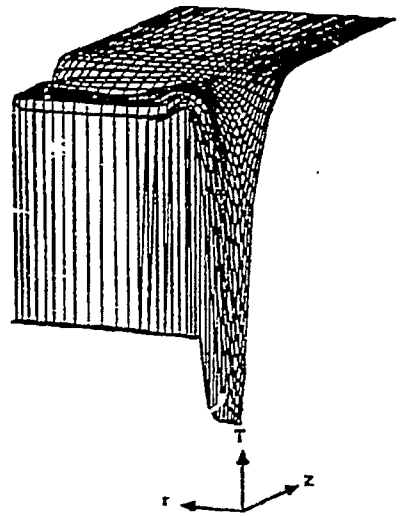

Figure III.A-4. Gas temperature isotherms and surface plots for gasification case.

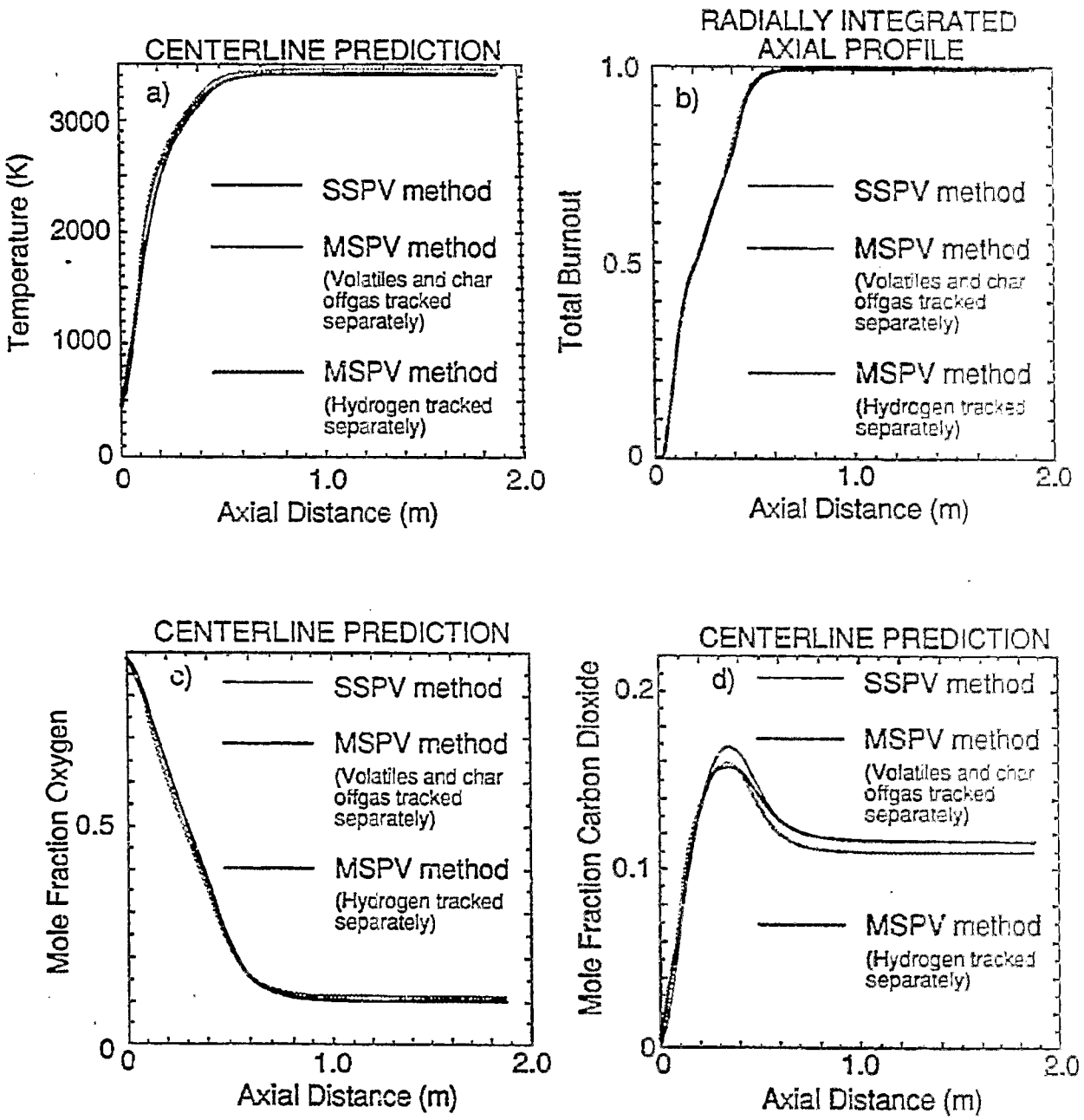

Figure III.A-5. Axial profiles for gasification case.

of the reactor is explained by the lower carbon content of the early offgas in the MSPV method. The lower value in the aft region of the reactor for the MSPV method tracking hydrogen separately is not yet understood, although it is probably related to the slightly higher temperature that was found in this case. After burnout and mixing are complete, the final temperature should be identical for all three cases for an adiabatic reactor, and so it may be that the cases were not converged tightly enough. Investigation of this apparent discrepancy is continuing.

The effects of ultimate volatile yield and external heat loss were also investigated. Centerline temperature for the gasification case is plotted for both 40 and 80 percent ultimate volatile yield in Figure III.A-6. The calculations shown in Figures III.A-4 and 5 assume an adiabatic reactor, but those in Figure III.A-6 assume a uniform heat loss of 20 percent throughout the reactor. Hence, the final temperatures are lower than those shown in Figure III.A-5. Also, the MSPV calculations were performed with volatiles and char offgas being tracked separately.

As expected, the temperature increases more rapidly with a volatile yield of 80 percent compared with 40 percent, because material is evolving at a higher rate from the coal. The differences between the SSPV and MSPV methods are small for 40 percent yield and even less for 80 percent yield. The reason for this result is the increased fraction of carbon that is devolatilized. At 40 percent volatile yield, and with the assumption of pure carbon for the char, all of the hydrogen, oxygen, nitrogen, and sulfur in the coal, as well as a portion of the carbon, was devolatilized. At 80 percent yield, a larger fraction of the carbon was devolatilized, thus increasing the carbon content of the volatiles, and decreasing the composition difference between the volatiles and the char offgas. In addition, the mass split between the two offgas fractions was heavily weighted toward the volatiles. The maximum difference between the SSPV and MSPV methods will occur when the composition of the two offgas fractions are as different as possible, and their relative masses are approximately equal. This maximum will be a function of the coal composition and the offgas fraction definitions, but is expected to occur at a volatile yield of approximately 50 percent when volatiles and char offgas are tracked separately.

The effect of heat loss is shown in Figure III.A-7. Fifty percent heat loss is thought to be representative of the actual heat loss of the BYU coal gasifier, although in a laboratory gasifier, the heat loss won t occur uniformly throughout the reactor as was assumed here. The assumption of uniformity in heat loss was made to simplify the calculations. As shown, the SSPV and MSPV methods may differ when external heat loss is taken into account, even though they are indistinguishable for an adiabatic reactor.

From the above, it is concluded that variability in coal offgas composition can have a significant impact on comprehensive code predictions for turbulent flames, particularly in slightly fuel-lean combustion simulations, and allowance should be made for taking this variability into account in codes incorporating detailed devolatilization submodels. The effects of this variability can be explained in terms of variability in the elemental composition and heating value. Variability in both elemental composition and heating value can be taken into account by a straightforward extension of the coal gas mixture fraction model for a locally adiabatic reactor, assuming statistical independence of the progress variables. Variability in heating value alone (constant elemental

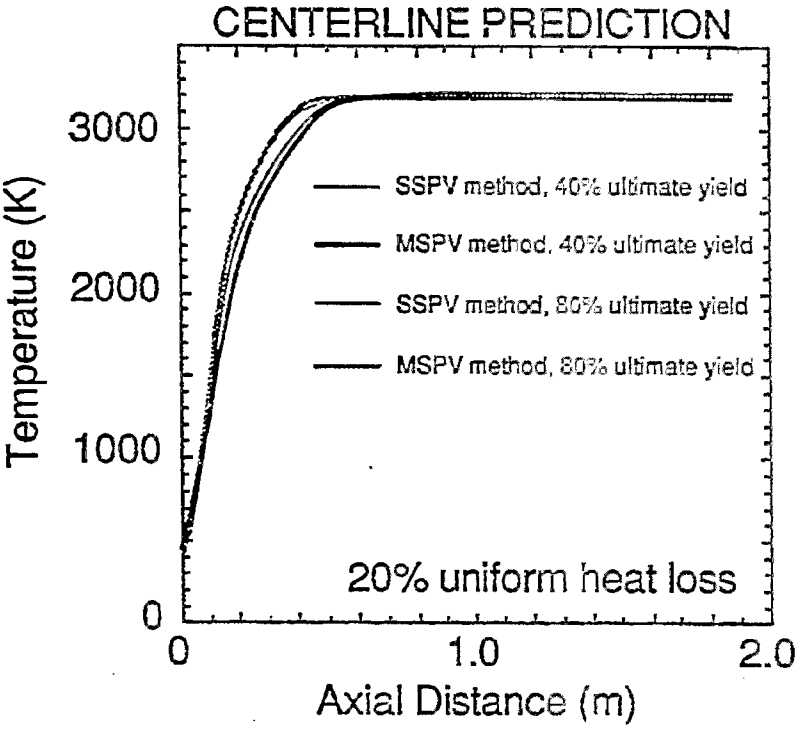

Figure III.A-6. Effect of ultimate yield on comparison between SSPV and MSPV methods.

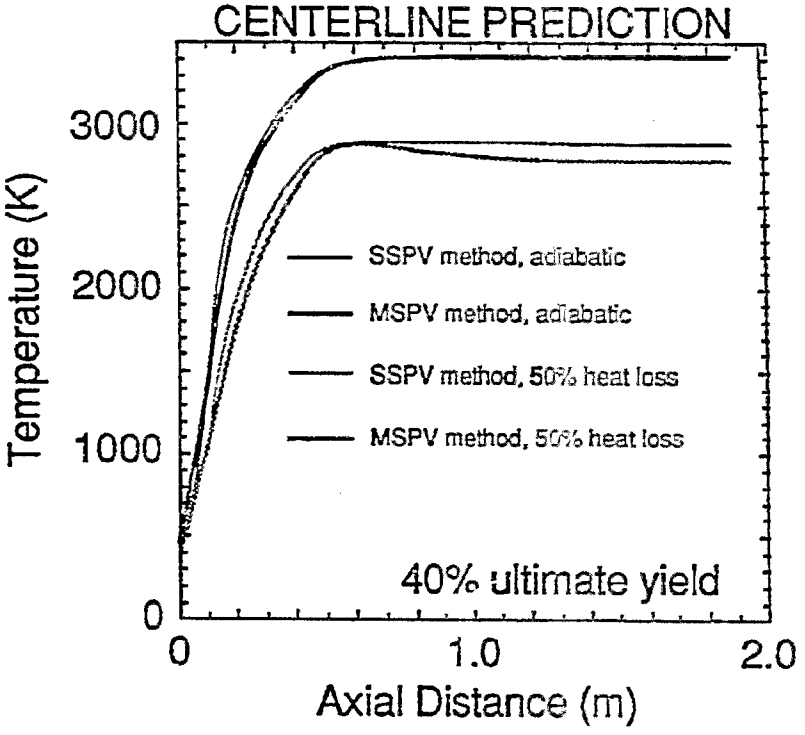

Figure III.A-7. Effect of external heat loss on comparison between SSPV and MSPV methods.

composition) can be taken into account with the existing single-variable approach if the energy equation is solved. In the former case, the effects of external heat loss can be approximated by a uniform heat loss factor. In the latter case, external heat loss is not assumed to be uniform. More research is needed to determine the number of variables that are needed and how the offgas components should be defined in the case of multiple variables.

Comparison of Coal Reaction Submodels - Table III.A-1 presents a comparison of the FG/DVC model and the Chemical Percolation Devolatilization (CPD) model (Grant et al., 1988). The purpose of the comparison is to gain insight into both model formulations and to find areas for mutual improvement. As mentioned in the previous quarterly report, the CPD model can be improved by including a transport model, including an explicit expression for available hydrogen, and incorporating molecular weight distributions. Two potential contributions of the CPD model are percolation lattice statistics and solid state NMR analytical data. Percolation theory is used for lattice statistics. When applied to Bethe lattices, percolation theory can be used to obtain algebraic solutions to lattice statistics. Algebraic solutions are approximately 5 orders of magnitude faster than Monte Carlo methods (Grant and Pugmire, 1988). The coding consists of less than 300 lines of Fortran. Solid State NMR can be used to obtain selected input parameters. The technique gives the ratio of bridge molecular weight to monomer molecular weight. From this information, the number of bridges can be calculated. The technique also gives the coordination number used for the Bethe lattice statistics.

Component 2 - Incorporating Improved Numerical Solution Methods

The purpose of this component of the subtask is to incorporate applicable improved numerical solution techniques that are being developed under separate funding by Smith and coworkers (Smith and Smoot, 1988) in this laboratory. These numerical techniques are described in the Second Annual Report of the Advanced Combustion Engineering Research Center (Smoot et al., 1988). Progress during the last year is summarized below.

Two specific methods have been under examination: multigrid techniques and coupled algorithms. Only the multigrid techniques are being considered for incorporation into PCGC-2 at the present time. The goal of the multigrid techniques is to make the amount of computational work proportional to the amount of real physical changes that are occurring in the solution. This is accomplished by dynamically moving the solution between grids of varying resolution, thus allowing most of the computationally expensive work to be performed on coarse grids and reducing the error components on the finer grids. During the last year, both axisymmetric, 2-D and Cartesian, 3-D fluid-dynamics codes have been developed based on multigrid techniques. Convergence to the level of truncation has been obtained at convergence rates that are at least ten times faster than without multigrid methods. A comparison of convergence rates with and without multigridding is shown in Figure III.A-8.

Component 3 - Incorporating SO_x-NO_x Submodel

The aim of this subtask component is to incorporate the SO_x-NO_x submodel being developed under Subtask 2.g into the comprehensive code, and to extend the comprehensive code to include sorbent injection and sorbent chemistry. Work continued on incorporating thermal NO in PCGC 2 as described under Subtask 2.g.

Table III.A-1. Model Comparisons

	FG-DVC	CPD
Lattice statistics	Yes	Yes
Computational method	Monte Carlo	Percolation Theory
Source of analytical data	FTIR,FIMS	Solid State NMR
Gas Release Model	FG	FG (modified)
Crosslinking with charring	Yes	Yes
From reaction cage	No	Yes
From side chain free-radical substitution	Yes	No
Hydrogen dependent stabilization	Explicit	Implicit
Transport Model	Yes	No
Tar Termination	H_2 depletion	Labile bond depletion

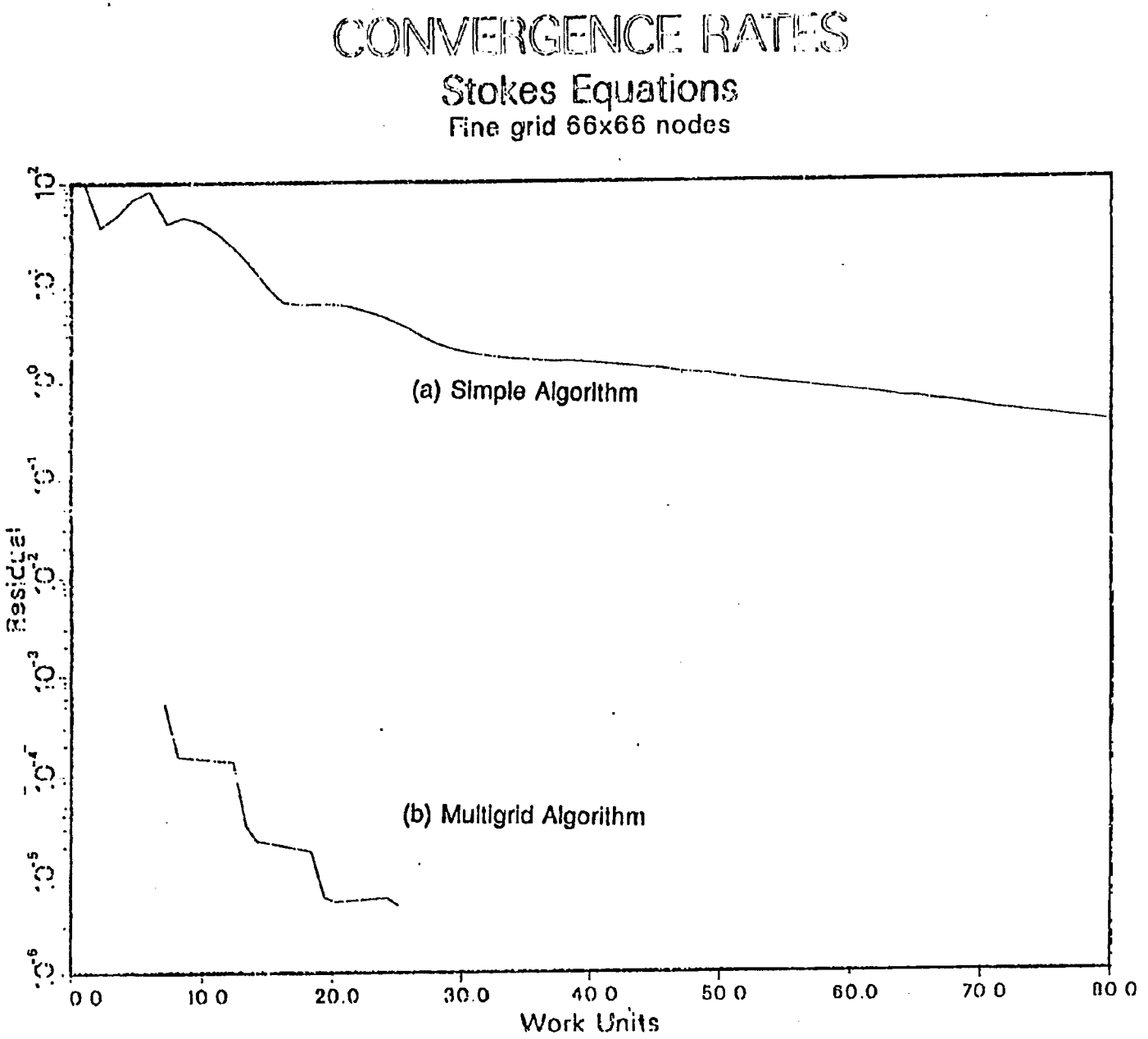

Figure III.A-8. Convergence rates of a set of two Stokes equations and a continuity equation with (b) and without (a) multigridding. (taken from ACERC Second Annual Report, Fig. 66)

The modification to include downstream injection of sorbent particles and their subsequent reactions with the gas phase is being based on independent work being performed by Pershing and coworkers at The University of Utah, where a sorbent chemistry submodel for fuel-lean conditions is being developed and incorporated into PCGC-2. Progress during the last year on the incorporation in PCGC-2 is described in the Second Annual Report of the Advanced Combustion Engineering Research Center (Smoot et al., 1988) and is summarized below.

An earlier version of PCGC-2 was modified by Pershing and coworkers to include injection of sorbent particles, and a series of calculations was performed to illustrate the overall computational procedure using the sorbent particle submodel developed at The University of Utah and described under Subtask 2.g. The results so far have illustrated the importance of sorbent dispersion on overall SO_2-capture effectiveness. This importance is illustrated in Figure III.A-9, which shows the predicted SO_2 concentration profile across the radius at the outlet of a full-scale utility boiler. The sorbent was injected at the centerline at a position 10 meters upstream from the exit. The pollutant concentration in the center of the duct is reduced significantly due to the presence of the sorbent. However, in this particular case, dispersion of the sorbent is inadequate and the concentration at the wall is essentially unaltered.

Component 4 - Implementing the Code on Computers

The aim of this component of the subtask is to implement the comprehensive code on several computers, including a workstation. This implementation will require, at a minimum, standardizing the source code so that it will run on a variety of computers. A user-friendly graphics interface is also desirable. During the quarter, two Sun workstations were made available to the project. The 1987 version of PCGC-2 is currently being adapted to run on those workstations.

Component 5 - Code Evaluation

The goal of this subtask component is to perform a statistical sensitivity analysis of input parameters to the improved code with advanced submodels and numerical methods incorporated under other components of this subtask. An existing databook will be used as a basis for the evaluation. No work was accomplished specifically under this subtask component during the past quarter.

Plans

During the next quarter, the FG/DVC submodel will be integrated into 87-PCGC-2, and calculations will be performed to compare code predictions with the FG/DVC submodel with those obtained with the simple two-step model. Calculations will also be performed with the FG/DVC submodel using one and two solids progress variables to further test the MSPV method. Solutions obtained with the energy equation will be used to determine the relative effects of varying elemental composition and enthalpy. A laminar version of PCGC-2 will be developed to assist AFR in analyzing data from their Transparent Wall Reactor. Independent work on numerical methods and modifications in PCGC-2 to include sorbent injection will continue to be monitored. 87-PCGC-2 with the integrated

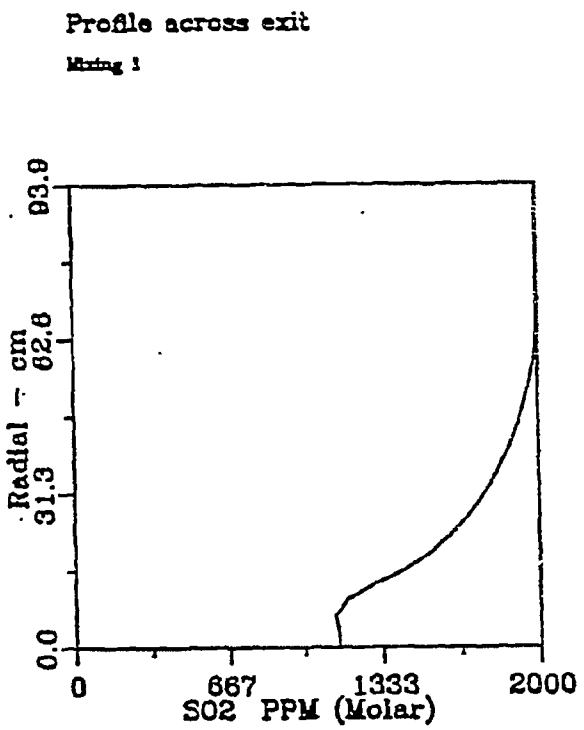

Figure III.A-9. Radical SO_2 profile at furnace exit (with sorbent particles). Sulfur concentration without sorbent is 2000 ppm. (Taken from ACERC Second Annual Report, Fig. 36.)

FG/DVC submodel will be installed on the Sun-3 workstation and a color graphics interface using the Uniras software will be developed.

III.B. SUBTASK 3.B. - COMPREHENSIVE FIXED-BED MODELING REVIEW, DEVELOPMENT, EVALUATION, AND IMPLEMENTATION

Senior Investigators - Sung-Chul Yi, Predrag Radulovic, B. Scott Brewster, and L. Douglas Smoot
Brigham Young University
Provo, Utah 84602
(801) 378-2076, 3097, 6240 and 4326

Objectives

The objectives of this subtask are: 1) to provide a framework for an improved fixed-bed model that can incorporate coal chemistry submodels, improved boundary conditions, and pollutant formation processes; and 2) to provide a basis for evaluating the model.

Accomplishments

Phase I of this subtask has two components: 1) A literature review and evaluation of existing fixed-bed coal gasification models and experimental data, and 2) development of a proposed advanced model. During the last quarter, work was initiated on an improved fixed-bed model that will serve as a basis for the advanced model. A preliminary review of literature correlations applicable to transport processes in fixed-bed reactors was completed. A set of momentum , mass, and heat transfer correlations was proposed for the improved fixed-bed model. Improvements, modifications and additions for the advanced fixed-bed model were identified.

Component 1 - Literature Review and Evaluation

This subtask component is aimed at 1) reviewing existing models for fixed-bed coal gasification to determine elements that might be used as a starting point for developing the advanced model, 2) determining appropriate correlations and submodels for physical properties of fixed beds, and 3) locating experimental data that can be used for model validation. The review of existing fixed-bed models was described in the First Annual Report (Solomon et al., 1987) and the 5th Quarterly Report (Solomon et al., 1987).

Review of Flow, Mass and Heat Transfer - Flow, mass and heat transfer processes in fixed bed gasifiers are very complex. Coarsely crushed coal settles while undergoing heating, drying, devolatilization, gasification and combustion. Polydisperse coal particles change diameter, shape and porosity. The coal bed permeability changes. There may be coal bridges, gas bubbles and channels. Gases flowing upward are heated and take part in a number of chemical reactions. Variations in bed permeability and possible formation of bubbles and channels also affect flow and pressure drop. Mass transfer occurs by diffusion and convection. Heat transfer is by conduction, convection and radiation in the gas and solid phases.

A summary of correlations recommended for an advanced fixed-bed model is presented in Table III.B-1. Plug flow will be assumed initially for the solid phase. Later, consideration will be given to the structural properties affecting the settling of coarse, crushed coal (Hauserman, 1984), and to the channeling effect in beds with variable permeability (Vafai, 1986). The

Table III.B-1. Flow, Mass and Heat Transfer Coefficients in Moving-Bed Reactor

Eq. No.	Coefficients	Correlations	References
(III.B-1)	Friction factor for gas phase	$f = \frac{1-\phi}{\phi^3}\left(1.75 + 150\,\frac{1-\phi}{Re}\right)$ for $\frac{Re}{1-\phi} < 500$	Ergun (1952)
(III.B-2)	Particle-to-fluid mass and transfer coefficient	$k_{g,i} = \frac{1.66G}{M_m p f_{a,i}} Re^{-0.51} Sc^{-2/3}$ for $Re < 190$, $\phi = 0.37$ spheres $k_{g,i} = \frac{0.983G}{M_m p f_{a,i}} Re^{-0.91} Sc^{-2/3}$ for $Re > 190$, $\phi = 0.37$ spheres	Froment and Bischoff (1979)
(III.B-3)	Particle-to-fluid heat transfer coefficient	$h_p = \frac{2.06 f C_p G}{\phi} Re^{-0.575} Pr^{-2/3}$	Gupta and Thodos (1963)
(III.B-4)	Effective axial diffusivity	$D_{ax} = \frac{U_{g,a} d_p}{1.5}$ $D_{ax} = \frac{U_{g,a} d_p}{1.5}$	Froment and Bischoff (1979)
(III.B-5)	Effective radial diffusivity	$D_{ar} = \frac{U_{g,r} d_p}{7\left[1 + 46\,(d_p/D_f)^2\right]}$	Froment and Bischoff (1979)
(III.B-6)	Effective axial conductivity	$K_a = K_{ea}^s + K_g \delta_1 PrRe$ for $Re < 50$ $K_a = K_{ea}^s + K_g\left(\delta_1 PrRe + \delta_2 Pr^2 Re^2 \frac{1}{\frac{K_{ea}^s}{K_g} + \delta_1 PrRe}\right)$ for $Re > 50$	Yagi et al. (1960); Bischoff (1962)

Table III.B-1. Flow, Mass and Heat Transfer Coefficients in Moving-Bed Reactor
(Continued)

Eq. No.	Coefficients	Correlations	References
(III.B-7)	Effective radial conductivity	$K_r = K_g[\phi(1+\beta\frac{h_{rv}d_p}{K_g}) + \frac{(1-\phi)\beta}{\frac{1}{\frac{h_p d_p}{K_g} + \frac{1}{\chi} + \frac{h_{rs}d_p}{K_g}} + \gamma\frac{K_g}{K_s}}] + K_g\frac{PrRe}{Pe_r}$	Froment and Bischoff (1970)
(III.B-8)	Effective radial gas conductivity	$K_{gr} = K_g[\phi(1+\beta\frac{h_{rv}d_p}{K_g}) + \frac{PrRe}{Pe_r}]$	DeWasch and Froment (1971)
(III.B-9)	Effective radial solid conductivity	$K_{sr} = K_g[\frac{(1-\phi)\beta}{\frac{1}{\frac{h_p d_p}{K_g} + \frac{1}{\chi} + \frac{h_{rs}d_p}{K_g}} + \gamma\frac{K_g}{K_s}}]$	DeWasch and Froment (1971)
(III.B-10)	Bed-To-wall effective heat transfer coefficient	$h_w = 2.44\frac{K^s_{gr}}{D_t^{4/3}} + 0.033\frac{K_g PrRe}{d_p}$	DeWasch and Froment (1971)
(III.B-11)	Bed-to-wall heat transfer coefficient for gas phase	$h^g_w = \frac{K_{gr}}{K_{gr} + K_{sr}}h_w$	DeWasch and Froment (1971)
(III.B-12)	Bed-to-wall heat transfer coefficient for solid phase	$h^s_w = \frac{K_{sr}}{K_{gr} + K_{sr}}h_w$	DeWasch and Froment (1971)

friction factor for the gas phase will be calculated by Ergun's equation (1952). MacDonald et al. (1979) have recently compared the Ergun equation with a large number of experimental data, and concluded that the Ergun equation is superior to others proposed in the literature for the wide porosity ranging from 0.36 to 0.92, whereas other equations are better for narrower porosity ranges. The problems of non-isothermal reacting flow with variable porosity and channeling remain to be investigated.

The particle-to-fluid mass transfer coefficient is correlated by Froment and Bischoff (1979). Alternatively, correlations are suggested by Gupta and Thodos (1963) and used by Denn et al. (1982) and Bhattacharya et al. (1986). The influences of porosity and asphericity remain to be determined. The particle-to-fluid heat transfer coefficient can be estimated by Gupta and Thodos' correlation (1963). Initially, the particles will be assumed to be uniform throughout. Later, intraparticle mass and heat transfer will be considered. Effective axial and radial diffusivities are correlated by Froment and Bischoff (1979), and by DeWasch and Froment (1971), respectively. Turbulent diffusion is assumed to be dominant in both directions.

Effective axial and radial conductivities are correlated by Yagi et al. (1960) and Bischoff (1962), and by Froment and Bischoff (1979), respectively. Both the axial and radial effective conductivities take into account molecular as well as turbulent contributions. The effective radial conductivity accounts for radiation. It should be noted that both correlations lump the gas and the solid phases together. There is no available information on the effective axial conductivities of the gas and the solid phases separately. The gas and solid phase contributions to the effective axial conductivity may be determined by analogy to the effective radial conductivity, if needed. Yagi et al. (1960) noted that at low flowrates, axial conductivity cannot be neglected. The effective conductivity is also given by Rohsenow et al. (1985). The effective radial conductivities of the gas and solid phases are correlated by DeWasch and Froment (1971). The same modes of the heat transfer are taken into account as for the lumped conductivities. Later, a diffusion approximation for radiative heat transfer will be considered.

The effective bed-to-wall heat transfer coefficient as well as the gas and solid phase contributions are determined by the correlations suggested by DeWasch and Froment (1971). The heat transfer to the wall is treated by Yagi and Wakao (1959) and Yagi and Kunii (1960). Additional information is given by Rohsenow et al. (1985). There are no direct experimental data available on the gas and the solid phase contributions to the bed-to-wall heat transfer.

Review of Fixed-Bed Technology - This review is limited to fixed-bed gasification. Stoker boilers are not considered. Fixed-bed gasification is one of two leading technologies for 1) production of fuel gas from coal, 2) integrated gasification, combined-cycle electrical power generation (IGCC), 3) production of synthesis gas from coal, and 4) retrofitting oil-fired power plants, fuel cells, etc. Fixed-bed gasification is the most important commercial gasification process. Eighty-nine percent of the coal that is gasified by fixed-bed (e.g. Lurgi), 10 percent by entrained-bed (e.g. Koppers-Totzek), and only 1 percent by fluid bed (e.g. Winkler). Lurgi's dry ash gasification process is the only commercial fixed-bed gasification process. Fixed-bed reactors may be conveniently divided into commercial, demonstration,

development, and laboratory units. Design and test data have been collected for some of these fixed-bed reactors, as summarized in Table III.B-2.

Component 2 - Detailed Plan for Fixed-Bed Model

This subtask component has already been completed.

Component 3 - Development of the Framework for an Advanced Fixed-Bed Model

The purpose of this component of the subtask is to develop a code framework for an advanced fixed-bed model. As a basis for this framework, an improved fixed-bed model is being developed. The improved fixed-bed model has many of the basic features of an advanced model, such as separate gas and solids temperatures, but is simplified in its treatment of chemistry and numerical solution method.

Improved Fixed-Bed Model - A simplified version of the advanced model incorporating separate gas and solids temperatures, but not including the advanced coal chemistry and bed hydrodynamic submodels planned for the advanced model has been formulated and is being coded. The improved model will provide a foundation for the advanced model to be developed later. The improved model is similar to the Washington University 2-D model (Bhattacharya et al., 1986), but is extended to include separate gas and solids temperatures, accumulation of energy and mass in the gas phase, radial dispersion of mass in the gas phase, and motion of the solid phase. Both drying and devolatilization have been assumed to occur instantaneously by previous investigators, since the time required for these two events is of the order of a few seconds compared to a total residence time of hours for the coal. In the advanced model, a detailed devolatilization submodel will be incorporated. Therefore, a segregated, but finite devolatilization zone is contemplated for the improved fixed-bed model. The particle submodel for this zone will not include all the details of heat and mass transfer, but it will be based on a rate expression such as the two-step model (Kobayashi et al., 1977; Ubhayakar et al., 1977). The residual char will be assumed to be pure carbon. Axial mixing of mass and energy will be assumed to be negligible based on the criterion developed by Young and Finlayson (1973). The dynamics of the gasifier are dominated by accumulation of mass and energy in the solid phase. Even though the residence time of the gases in the reactor is short, the accumulation term in the gas phase will be included due to the mathematical simplicity of the resulting equations. Solid velocity and bed porosity will be assumed to be constant.

The differential equation set for the improved moving-bed model is shown in Table III.B-3. The auxiliary equations are shown in Table III.B-4. The boundary conditions necessary to solve the partial differential equations system, Eqns. (III.B-13) through (III.B-19), are as follows:

1. Symmetry of the bed at the centerline

$$\left.\frac{\partial w_i}{\partial r}\right|_{r=0} = 0 \quad ; \quad \left.\frac{\partial T_s}{\partial r}\right|_{r=0} = 0 \quad , \quad \left.\frac{\partial T_g}{\partial r}\right|_{r=0} = 0 \qquad \text{(III.B-24)}$$

TABLE III.3-2

FIXED-BED REACTORS TEST DATA

Commercial

1. LURGI Dry Ash
   - Sasolburg and Secunda (SASOL), South Africa — not available
   - Westfield, Scotland 1974
     J. Stefano (1985) and Woodall-Duckham (1974).
     Effluent data, height of combustion zone, variations in coal type, some variations in operating parameters.
   - Beulah (Great Plains), North Dakota, 1984
     B.W. Benjamin (1984), I.H. Ringard and B.W. Benjamin (1985)
     Some design data, no experimental data.

Demonstration

1. BGC/LURGI Slagging Ash
   - Westfield, Scotland, 1981
     J.E. Scott (1981) and J. Stefano (1985).
     Effluent data, Pittsburgh No. 8 coal, some variations in operating parameters, solid flow problems, dynamic behavior, gas dust loading, excellent.

2. KILnGAS
   - Wood River Station, Illinois — not available

Development

1. METC - Morgantown, West Virginia
   - K. Prater (1986), J. Stefano (1985) and other METC publs.
     Effluent and some other data, variations in coal type, variations in operating conditions, O_2 vs. air, sophisticated measurements (CARS, etc.), the second most comprehensive set of data available.

2. MGU - Bristol, Virginia
   - C.I.C. Chu and B.L. Gillespie (1987)
     Some design data, no experimental data.

TABLE III.B-3

FIXED-BED REACTORS TEST DATA
(Continued)

Development (Continued)

3. Wellman-Galusha -- Minneapolis, Minnesota
   - D. Thimsen, et al. (1984, 1985), data book soon.
   Effluent data, many U.S. coals, axial profile data on a pressure and temperature, operational procedure, monitoring procedure, test procedure, calculation and data analysis procedure, all dimensions of gasifier, detailed data on measuring equipment, the most comprehensive set of data available.

4. GEGAS -- Schenectady, New York
   - K. J. Daniel and P.P. Shah (1980), J. Stefano (1985), Corman, et al. (1984).
   Effluent data only, some variations in operating parameters.

5. GFETC -- Grand Forks, North Dakota
   - J. Stefano (1985).
   Effluent data, height of combustion zone, some variations in operating conditions.

6. RUHR 100 -- Dorsten, West Germany — not available

7. KGN -- Hueckelhoven, West Germany — not available

Laboratory

1. Washington University -- St.Louis, Missouri
   - A. Bhattacharya, et al. (1986). A. Bhattacharya (1985), L. Salam (1983).
   Effluent data, axial temperature profile, unsteady data.

2. Pennsylvania State University -- University Park, Pennsylvania
   - A. Barriga and R. H. Essenhigh (1980), T. Eapen, et all. (1977), T. Eapen (1979)
   Effluent data, axial temperature and gas composition profiles.

Table III.B-3. Summary of Model Differential Equations for Improved Fixed-Bed Model

Eq. No.	Type	Equation
(III.B-13)	Gas species mass balance	$\frac{\partial w_i}{\partial t} = -v_g \frac{\partial w_i}{\partial z} + \frac{1}{r}\frac{\partial}{\partial r}(r)^i_{eff}\frac{\partial w_i}{\partial r}) + \frac{1}{\phi\rho_g}(S_{g,i} - w_i S_T)$
(III.B-14)	Total gas mass balance	$\frac{\partial \rho_g}{\partial t} = -\frac{\partial (v_g \rho_g)}{\partial z} + \frac{S_T}{\phi}$
(III.B-15)	Total gas energy balance	$\frac{\partial T_g}{\partial t} = -v_g \frac{\partial T_g}{\partial z} - \frac{1}{C_{pg}}\left[\sum_j h^o_{g,j}(\frac{\partial w_j}{\partial t} + v_g \frac{\partial w_j}{\partial z})\right] + \frac{1}{\phi\rho_g C_{pg}}\left[\frac{1}{r}\frac{\partial}{\partial r}(r\phi K_{gr}\frac{\partial T_g}{\partial r}) + Q_T + \sum_j S_{g,j}h_{g,j} - h_g S_T\right]$
(III.B-16)	Solid species mass balance	$\frac{\partial y_i}{\partial t} = v_s \frac{\partial y_i}{\partial z} + \frac{(S_{c,i} - w_i S_T)}{(1-\phi)\rho_c}$
(III.B-17)	Total solid mass balance	$\frac{\partial \rho_c}{\partial t} = v_s \frac{\partial \rho_c}{\partial z} + \frac{S_T}{(1-\phi)}$
(III.B-18)	Total solid energy balance	$\frac{\partial T_s}{\partial t} = v_s \frac{\partial T_s}{\partial z} + \frac{1}{(1-\phi)\rho_c C_{pc}}\frac{1}{r}\frac{\partial}{\partial r}(r(1-\phi)K_{sr}\frac{\partial T_s}{\partial r}) + \frac{1}{(1-\phi)}(-Q_T - \sum_j S_{s,j}h_{s,j})$
(III.B-19)	Gas momentum equation	$\frac{\partial v_g}{\partial z} = \frac{\sum_j \frac{1}{M_j}(\frac{\partial w_j}{\partial t} + v_g\frac{\partial w_j}{\partial z})}{\sum_j (\frac{w_j}{M_j})} + \frac{1}{T_g}(\frac{\partial T_g}{\partial t} + v_g\frac{\partial T_g}{\partial z}) + \frac{S_T}{\phi\rho_g}$

Table III.B-4. Auxilliary Equations for Improved Fixed-Bed Model

Eq. No.	Type	Equation
(III.B-20)	Heat transfer between solid and gas phases	$Q_T = h_p \frac{6(1-\phi)}{d_p} (T_s - T_g)$
(III.B-21)	Ideal gas law	$\frac{p}{R} = \rho_g T_g \sum_j (\frac{w_j}{M_j})$
(III.B-22)	Total gas phase enthalpy	$h_g = \sum_j w_j h^o_{g,j} + \int_{T_o}^{T_g} C_{pg} dT$
(III.B-23)	Total gas phase production	$S_T = \sum_l S_{s,l}$

2. No penetration of mass through the wall

$$\left.\frac{\partial w_i}{\partial r}\right|_{r=R} = 0 \qquad \text{(III.B-25)}$$

3. No heat accumulation at the wall

$$K_{gr}\left.\frac{\partial T_g}{\partial r}\right|_{r=R} = h_{wg}(T_{g,b} - T_w) \quad , \quad K_{sr}\left.\frac{\partial T_s}{\partial r}\right|_{r=R} = h_{ws}(T_{s,b} - T_w) \qquad \text{(III.B-26)}$$

The temperature of water inside the water jacket, T_W, is taken to be constant at 490 K. This is the saturation temperature of steam at system pressure.

4. The operating input conditions

$$\text{at z=0,} \quad w_i = w_i(r, 0, t) \quad , \quad T_g = T_g(r, 0, t) \quad , \quad v_g = v_g(r, 0, t) \qquad \text{(III.B-27)}$$

$$\text{at z=L,} \quad y_k = y_k(r, L, t) \quad , \quad T_s = T_s(r, L, t) \qquad \text{(III.B-28)}$$

5. The initial conditions:

$$\text{at t=0,} \quad T_g = T_g^o(r, z, 0) \quad , \quad T_s = T_s^o(r, z, 0) \quad , \quad w_i = w_i^o(r, z, 0) \quad , \quad y_k = y_k^o(r, z, 0) \qquad \text{(III.B-29)}$$

The input properties, model parameters, dependent and independent variables are summarized in Table III.B-5.

The important reactions considered in the improved moving bed model are shown in Table III.B-6. The gasification reactions R1, R2, and R3 are considered reversible. The equilibrium constants for the reactions follow an Arrhenius form:

$$K_i = K_i^o \exp\left(-\frac{\Delta H_i^o}{RT_g}\right) \qquad \text{(III.B-30)}$$

The intrinsic reaction rates of reactions R1 through R5 are assumed to follow the mass action law, and the rate constants have Arrhenius form:

Table III.B-5. Model parameters and variables

Input Data

Gas velocity (v_g)	Solid Velocity (v_s)
Gas composition (w_i)	Solid species composition (y_k)
Gas temperature (T_g)	Solid temperature (T_s)
Pressure (P)	Wall temperature (T_w)

Reactor Parameters

Dimensions (diameter, length)	Operating conditions

Independent Variables

Physical coordinates (r, z)	time (t)

Dependent Variables

Gas velocity (v_g)	Gas composition (w_i)
Gas temperature (T_g)	Solid temperature (T_s)
Pressure (P)	Wall temperature (T_w)
Extent of reaction ($S_{s,i}$, S_T)	Solid species composition (y_k)

Table III.B-6. Major reactions occurring in the gasifier[a]

$C + H_2O \rightarrow CO + H_2$	(R1)
$C + CO_2 \rightarrow 2CO$	(R2)
$C + 2H_2 \rightarrow CH_4$	(R3)
$C + kO_2 \rightarrow (2-2k)CO + (2k-1)CO_2$	(R4)
$C + H_2O \rightarrow CO_2 + H_2$	(R5)

[a]Gasification, reactions 1-3, Combustion, reaction 4, Water-gas shift, reaction 5.

Table III.B-7. Reaction Parameters for Illinois and Wyoming Coal

Reaction	$k^o_{r,i}$ (kPa hr)	$E_i \times 10^{-5}$ (kJ/kmol)	Reference
R1			
Illinois	2.178×10^4	1.757	Cho (1980)
Wyoming	1.464×10^4	1.465	Yoon et al. (1978)
R3			
Illinois	1.465×10^{-4}	0.6716	*
Wyoming	2.931×10^{-4}	0.6716	Cho (1980)
R4			
Illinois	6.360×10^7	1.13	Cho (1980)
Wyoming	6.360×10^7	1.13	Cho (1980)

* "No data are available in the literature"
k^o_r is assumed as one half of that of Wyoming coal
$k_{r,co2}$ was assumed as 0.6 $k_{r,H2O}$ (Yoon et al., 1978)

Table III.B-8. Equilibrium parameters

	Equilibrium Parameters		
Reaction	K^o_i	ΔH^o_i(kcal/mole)	Reference
R1	3.098×10^7	32.457	Yoon et al. (1978)
R2	1.222×10^9	40.300	Yoon et al. (1978)
R3	1.472×10^{-6}	-21.854	Yoon et al. (1978)
R4	infinite	(irreversible)	
R5	0.0265	-7.860	Yoon et al. (1978)

$$k_{r,i} = k_{i,o}\exp(-\frac{E_i}{RT_g}) \qquad \text{(III.B-31)}$$

The kinetic parameters depend upon the specific type of coal used. An Illinois No. 6 bituminous coal has comparatively low reactivity while a Wyoming subbituminous coal has comparatively high reactivity. The kinetic and equilibrium parameters for these two coals are listed in Tables III.B-7 and 8. In the char-oxygen reaction, the main difficulty is in predicting the molar ratio of CO to CO_2 produced. In this work, a relation of the form

$$\frac{CO}{CO_2} = k\exp(-\frac{E}{RT_g}) \qquad \text{(III.B-32)}$$

proposed by Rossberg (1956) is being considered.

The split boundary value problem resulting from the mass and energy balances for countercurrent flow may be solved by many methods. The simplest approach is to use a shooting method in which equations are integrated from the bottom to the top using a marching type integration method. While this method worked well for the homogeneous case (Yoon et al. 1978), it was disastrous for the heterogeneous model. Amundson and Arri (1978) also reported similar difficulties. In an attempt to overcome this difficulty, a dynamic model was suggested. The system of simultaneous partial differential equations thus has three dimensions: axial position, radial position and time, and each dimension must be treated separately. For the improved model, orthogonal collocation is being used for the radial dimension, with finite differencing in the time domain (Bhattacharya et al., 1986). The resulting set of ordinary differential equations will be integrated using Gear's routine (Gear, 1971).

Plans

A computer code will be developed for the improved fixed-bed model as a foundation for the advanced model. The improved fixed-bed model will be completed and exercised. Concurrent with the development of the improved fixed-bed model, the particle reaction submodel requirements will be determined. Development of the numerical solution method will be initiated.

Nomenclature

C_p	local gas phase heat capacity [kJ/kgmol K]
C_{pg}	total gas phase heat capacity [kJ/kgmol K]
C_{pc}	total solid phase heat capacity [kJ/kgmol K]
D_{ieff}	effective radial gas diffusivity of species i [m^2/hr]
D_f	diameter of the reactor [m]
D_{ea}	effective axial diffusivity [m^2/hr]
D_{er}	effective radial diffusivity [m^2/hr]
d_p	particle diameter [m]
E_i	activation of energy of reaction i [kJ/kgmol]
F_G	total molar flux of gas stream [kgmol/m^2 hr]
f	pressure drop
f	proportionality factor for the gas-solid heat transfer coefficient of the coal bed
G	mass flux of the gas stream [kg/m^2 hr]
h_p	gas-solid heat transfer coefficient of the coal bed [kJ/m^2 hr K]
h_{rw}	heat transfer coefficient for thermal radiation, void space to void space [kJ/m^2 hr K]
h_{rs}	equivalent radiation heat transfer coefficient for the solid phase [kJ/m^2 hr K]
h_w	homogeneous bed-to-wall effective heat transfer coefficient [kJ/m^2 hr K]
h_{gw}	effective wall heat transfer coefficient for gas phase [kJ/m^2 hr K]
h_{sw}	effective wall heat transfer coefficient for solid phase [kJ/m^2 hr K]
h_g	total enthalpy of gas phase [kJ/kgmol]
$h_{g,j}$	enthalpy of gas species j [kJ/kgmol]
h_p	particle-to-particle contact heat transfer coefficient [kJ/m^2 hr K]
K_a	effective axial thermal conductivity [kJ/hr m K]
K_{sea}	static contribution of effective radial thermal conductivity [kJ/hr m K]
K_{gsea}	static contribution of effective axial gas thermal conductivity [kJ/hr m K]
K_g	gas thermal conductivity [kJ/hr m K]
K_{gr}	effective radial gas conductivity [kJ/hr m K]
K_{sr}	effective radial solid conductivity [kJ/hr m K]
K_s	solid thermal conductivity [kJ/hr m K]
K	pre-exponential factor
$k_{r,i}$	intrinsic reaction rate of species i [kmol/kmol char kPa hr]
$K_{or,i}$	Arrhenius constant for intrinsic reaction rate of species i [kmol/kmol char kPa hr]
K_i	equilibrium constant of reaction i
K_{oi}	pre-exponential factor in equilibrium constant of reaction i
$k_{g,i}$	mass transfer coefficient of gaseous species i through bulk film
L	reactor length [m]
M_j	molecular weight of species j [kg/kgmol]
M_w	mixture molecular weight of species [kg/kgmol]
P	total pressure [kPa]
Pe	Peclet number
P_i	partial pressure od gas species i [kPa]
$P_{fa,i}$	film pressure factor of species i
Pr	Prandtl number

Q_T heat transfer between gas and solid phase [kJ/m^3 hr]
r radial direction [m]
R reactor radius [m]
R universal gas constant
Re Reynolds number
S_c total solid phase source per volume of bed [kg/m^3 hr]
$S_{c,k}$ solid species k source per volume of bed [kg/m^3 hr]
$S_{s,i}$ species i gas source per volume of bed by heterogeneous reaction [kg/m^3 hr]
S_T total gas phase source per volume of bed [kg/m^3 hr]
Tg gas phase temperature [K]
T_s solid phase temperature [K]
T_w wall temperature [K]
t time, [hr]
U_g superficial gas velocity [m/hr]
$U_{g,a}$ superficial axial gas velocity [m/hr]
$U_{g,r}$ superficial radial gas velocity [m/hr]
v_g interstitial gas velocity [m/hr]
v_s effective solid velocity [m/hr]
w_i weight fraction of gas species i
y_k weight fraction of solid species k
z axial direction [m]

Greek symbols

β effective length between centers of neighboring solid particles divided by equivalent diameter of the particles
χ effective thickness of the fluid film adjacent to the surface of two solid particles divided by equivalent diameter of the particles
$\delta 1$ parameter in effective axial conductivity
$\delta 2$ parameter in effective axial conductivity
γ effective length of a clogged particle for heat transfer divided by the equivalent diameter of the particle
ε emissivity of the solid
ϕ bed porosity
ρc total solid density [kg/m^3]
ρg total gas density [kg/m^3]
ϕ total bed porosity

Superscripts
o Initial condition